Hydrodynamic Stability of Hypersonic Chemically Reacting Boundary Layers II

Olaf Marxen
Department of Mechanical Engineering Sciences
Faculty of Engineering and Physical Sciences
University of Surrey
Guildford, Surrey GU2 7XH
United Kingdom

o.marxen@surrey.ac.uk

ABSTRACT

In these notes, an introduction to non-linear hydrodynamic instability in the presence of high-temperature gas effects is given. Focus is put on high-temperature gas effects, including chemical reactions, on weakly non-linear boundary-layer instability. Strongly non-linear effects are only considered for a frozen gas. Results have been obtained from numerical simulations of configurations in which the temperature at the boundary-layer edge is low, whereas the temperature inside the boundary layer may be very high. This case may be regarded as representative for laminar-turbulent transition on the surface of slender bodies.

At high Mach numbers, linear acoustic instability leads to the strong streamwise growth of two-dimensional waves, which eventually attain large amplitudes. These waves initiate wave breakdown, caused by the secondary instability of the boundary layer. For moderately reactive flows, the effect of chemical reactions on the secondary instability is found to be very similar to the effect of cooling at the wall. The same observation has been made already for the base flow as well as for linear perturbations. As a result of this cooling effect, the primary wave attains higher amplitudes, which in turn increases the amplification rate of secondary oblique waves. No direct effect of chemical reactions on the secondary instability mechanism could be observed. Fundamental resonance, in which both the primary and the secondary wave possess the same frequency, is found to be more important than subharmonic resonance for the high Mach number considered.

Strongly nonlinear effects cause a reduction of primary as well as secondary amplification. At the stage when these effects set in, both primary and secondary disturbances have a similar amplitude. Evidence for the emergence of shocklets is during this stage found.

Contents

1.0 NON-LINEAR BOUNDARY-LAYER INSTABILITY AND TRANSITION TO TURBULENCE

1.1 Introduction to Non-Linear Boundary-Layer Instability

A prerequisite to predicting the transition location is the knowledge of transition mechanisms. However, many fundamental aspects and breakdown mechanisms of the laminar-turbulent transition process in high-speed boundary layers have not yet been studied in detail. While theoretical approaches provide valuable insight into the flow dynamics, the quantitative effects of the assumptions of linearity and parallel flow often used in theories need to be understood.

Numerical methods based on a high-order discretization are particularly well suited for simulations of transition because of the low dispersion and dissipation introduced that preserve the character of the underlying flow. However, as pointed out in Ref. [1], the additional complexity associated with the combination of high Mach numbers and high temperatures causes the gas to no longer behave as a calorically perfect gas, which makes such simulations challenging. At present, not many high-order numerical methods are capable of handling non-linear instability waves in the high-temperature regime.

The three stages of the transition process have been introduced in Ref. [1]. The second stage, amplification of small linear perturbations, has been studied using linear stability theory [2, 3] as well as the parabolized stability equations [4], including high-temperature gas effects [5, 6] as discussed in Ref. [1]. Two different types of linear instability are known to play a role at very large Mach numbers. The first is an inviscid instability caused by a generalized inflection point (first-mode or inflectional instability). The second is an inviscid instability due to the presence of relative supersonic flow in the boundary layer (second-mode, acoustic or Mack instability).

Once the linearly amplified perturbations have grown to large amplitudes, non-linear effects set in [7] and oblique breakdown [8] or secondary instability [9] may occur, the latter in the form of fundamental or subharmonic resonance [10]. For Mach numbers exceeding a value of at least five, two-dimensional second-mode disturbances are expected to reach large amplitudes first, since they are known to be most amplified at high Mach numbers. This suggests that oblique breakdown will play a minor role. Instead, subharmonic or fundamental resonance in the presence of a large amplitude two-dimensional wave may cause breakdown to turbulence.

A number of studies have been performed of non-linear boundary-layer instability and transition at very high Mach numbers. Ref. [11] carried out experimental investigations of non-linear transitional stages for high Mach numbers, but they did not take into account chemical reactions due to low temperatures in the

boundary layer occurring in their investigations. The same is true for the numerical investigations of Ref. [12]. For flows with high-temperature gas effects, non-linear breakdown to turbulence has mostly been considered experimentally, e.g. in Ref. [13] or more recently in Ref. [14]. Still, our knowledge of the non-linear transitional stages remains very limited.

1.2 Wave Breakdown

As it has been described in Ref. [1], we can distinguish between two general routes of non-linear breakdown: wave and streak breakdown. Breakdown to turbulence is initiated when the primary flow structure, the wave or the streak, reaches a large amplitude and creates a new, secondary instability.

In the case of wave breakdown, non-linear waves assume the form of spanwise vortices and are susceptible to additional instabilities. For streak breakdown, the wall-normal or spanwise gradients of the streamwise velocity profile initiate a localized shear-layer instability, often leading to a varicose or sinuous motion of the low-speed streak. In these notes, we will only consider wave breakdown.

The linear amplification of streamwise traveling waves eventually leads to the presence of large-amplitude waves in the boundary layer. Depending on the flow field under consideration, higher harmonics of these waves develop and, together with the main wave, form coherent structures. In boundary layers the presence of a large-amplitude traveling wave only is sufficient to induce secondary instability.

As a result of these so-called primary waves, a weakly non-linear mechanism may become active in the boundary layer: the unsteady secondary instability. Once this primary perturbation possesses a sufficiently large amplitude, the growth of oblique secondary waves may be significantly enhanced [10]. Apart from numerical simulations, secondary instability can be investigated theoretically using Floquet theory.

The secondary instability is independent of the amplitude of the secondary wave, and therefore it is only weakly non-linear. However, it parametrically depends on the amplitude of the primary wave. The secondary waves fall into resonance with the primary waves. A characteristic feature of this resonance is the synchronization of phase velocities of the primary and secondary waves. The latter adjusts its phase speed to match the one of the primary wave.

It is convenient to consider a pair of streamwise traveling waves. In a frame of reference moving with these two primary waves, they may be viewed as vortices. The type of linear instability mechanism of the primary waves is usually not important, and a non-linear primary wave can arise due to a Tollmien-Schlichting, Kelvin-Helmholtz, Lees-Lin, or a Mack instability.

The waves resulting from one of the secondary instability mechanisms may possesses half the frequency (subharmonic resonance) or the same frequency (fundamental resonance) as the primary waves. A comprehensive description of corresponding breakdown scenarios for (incompressible) boundary layers can be found in Refs. [10, 15].

The disturbance growth due to a secondary instability mechanism is typically very strong. For incompressible flow, the primary wave is often a two-dimensional wave, since such a wave is usually most amplified. For supersonic flow ($Ma_\infty \leq 2$), the onset of non-linear effects could be caused by secondary instability [fundamental or subharmonic resonance, see Refs. 7, 10] or oblique breakdown [7, 16]. For such a compressible boundary-layer flow at low supersonic Mach numbers, oblique waves are most amplified, and hence the primary wave may be an oblique wave. In this case, asymmetric secondary wave arrangements can be observed, an example is given in Ref. [9].

At higher Mach numbers, the fundamental instability may be stronger than subharmonic instability, as found in the investigations of Refs. [17, 18]. For hypersonic flow, the primary wave is two-dimensional again, since the Mack instability is strongest for these conditions. This will be discussed in more detail below, based

on results from Refs. [19, 20].

The occurrence of secondary instability leading to eventual breakdown to turbulence, may be influenced by thermal non-equilibrium effects even if the gas is too cold to dissociate [21]. Quantifying this influence will require both thermal equilibrium and non-equilibrium results, but it is beyond the scope of these notes.

1.2.1 Elliptic and Hyperbolic Instability

At least two different secondary instability mechanisms may occur for pairs of spanwise waves or vortices: elliptic [22] and hyperbolic [23, 24] instability. Elliptic instability leads to a three-dimensional deformation of the traveling waves and is the dominating instability in boundary layers. Hyperbolic instability can usually only be seen in separated flow or free-shear-layer transition, where it occurs in the stagnation-flow region between consecutive vortices, the so-called braid region, but it is unlikely to occur in hypersonic boundary layers.

1.2.2 Oblique Breakdown

Oblique breakdown is a special case, and it has been observed in both incompressible [25] and supersonic flows [8, 26]. In incompressible flow, a pair of decaying oblique traveling waves induces a pair of streamwise streaks by means of the lift-up effect, and then streak breakdown occurs.

For compressible flow, the pair of oblique traveling waves is growing, but streamwise streaks are still found to play an important role in the breakdown process. Oblique disturbances are most amplified in supersonic flow, and therefore oblique breakdown could be an important mechanisms in this regime. For larger Mach numbers, however, two-dimensional second-mode disturbances are stronger amplified for a calorically perfect gas [2] as well as for the case of a gas with high-temperature effects [27] as mentioned above. This suggests that oblique breakdown will play a lesser role and subharmonic or fundamental resonance in the presence of a large amplitude two-dimensional wave (of second-mode type) may cause breakdown to turbulence for high Mach numbers.

Oblique breakdown is most likely not relevant for the configurations considered here due to the very high freestream Mach number. However, this type of breakdown could be important for blunt bodies, even if they move at high Mach numbers.

1.3 Scope

The present notes are devoted to non-linear instabilities of hypersonic boundary layers with high-temperature gas effects. It is expected that the reader is familiar with Ref. [1]. As in that reference, we will again consider configurations in which the temperature at the boundary-layer edge is sufficiently low so that the gas in the freestream can be modeled as an calorically perfect gas, while the temperature inside the boundary layer may be very high. Configurations for which the opposite is true, i.e. high temperature in the freestream with wall cooling, are beyond the scope here.

In addtion to being familiar with what has been described in Ref. [1], in particular the definitions given therein, the reader should also be familiar with at least some aspects of non-linear instability theory applied to boundary layers, and Ref. [10] provides a good overview.

Below and in Ref. [1], we restrict ourselves to the discussion of basic physical effects with respect to linear and non-linear hydrodynamic stability, as they have been found from numerical simulations. Throughout these notes and in Ref. [1], we only consider fluids that are in thermal equilibrium.

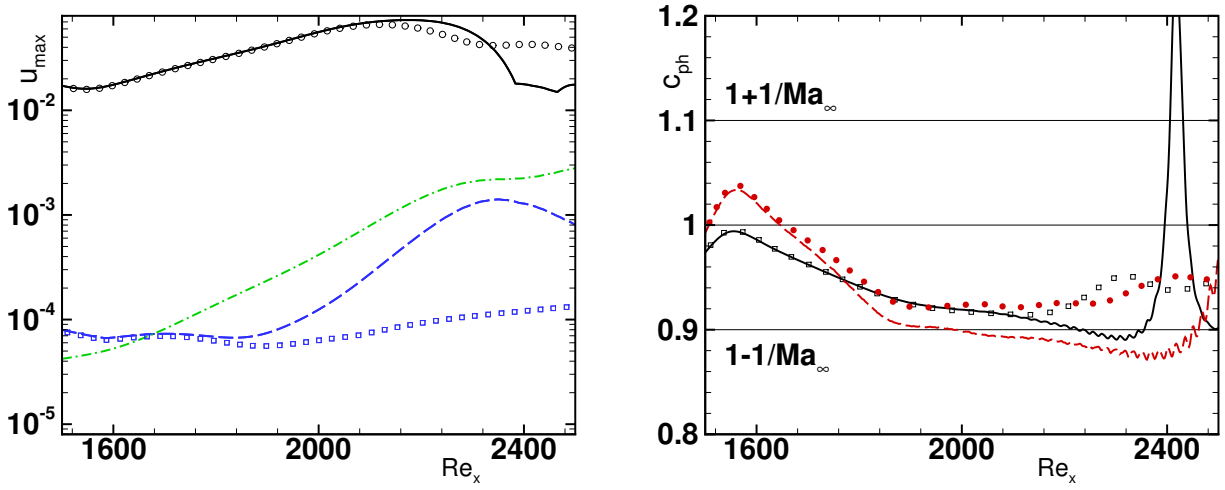

Figure 1: Left: Maximum amplitudes of the streamwise velocity ($A_v^{(1,0)} = 10^{-2}$, $A_v^{(1,\pm k)} = 10^{-4}$, $\Delta\Phi = \pi/4$) for frozen flow [19]. The most important modes during secondary instability: mode $(1,0)$ (solid line), $(1,\pm4)$ (dashed line) and $(0,4)$ (dash-dotted line) are depicted; scaled linear results (□) are given for reference. Right: Phase velocities for disturbance waves relevant for secondary instability (computed from the wall pressure). Mode $(1,0)$ (solid line), mode $(1,\pm4)$ (dashed line). Linear results (Mode $(1,0)$: □, mode $(1,\pm4)$: •) are given for reference.

2.0 WEAKLY NON-LINEAR DISTURBANCE EVOLUTION

2.1 Overview

The most important modes active during secondary boundary-layer instability and their parametric dependencies are examined below for fundamental resonance. The same conditions as in § 2.0 and § 3.0 of Ref. [1], case A, are used here and in the following. Two gas models are considered: frozen flow and finite-rate chemically reacting flow.

In the presence of a large-amplitude two-dimensional wave mode $(1,0)$ (solid line in figure 1, left), oblique waves of the same frequency, modes $(1,\pm4)$ given by the dashed line, are strongly amplified so that their growth significantly exceeds that seen in the absence of mode $(1,0)$ (symbols in the figure). A characteristic feature of fundamental resonance is the growth of a mode $(0,4)$ disturbance [10]. In the figure, such a mode (dash-dotted line) can be seen to grow together with modes $(1,\pm4)$. As the two unsteady waves fall into resonance, their downstream evolution also synchronizes. At the start of secondary growth ($Re_x \gtrapprox 1800$), the phase speed of the oblique waves decreases compared to the linear case (figure 1, right) and eventually also a decrease in phase speed is seen for the primary wave ($Re_x \gtrapprox 2100$). The phase velocities shown here have been computed as described in § 1 of Ref. [1].

It can also be observed in figure 1(left) that non-linearity destabilizes the primary wave, mode $(1,0)$. When comparing the solid line and the corresponding symbols for the two-dimensional disturbance in the figure we see that the large-amplitude wave (solid line) continues to be amplified further downstream, although this effect is small.

In order to better illustrate the development of the flow field during secondary instability, the streamwise evolution of velocity and thermodynamic components is inspected. Figure 2 provides an overview of the amplitude evolution for five different components for the primary (left) and secondary (right) disturbance. Except for the maximum density amplitude, all components grow strongly during the stage of secondary instability (figure

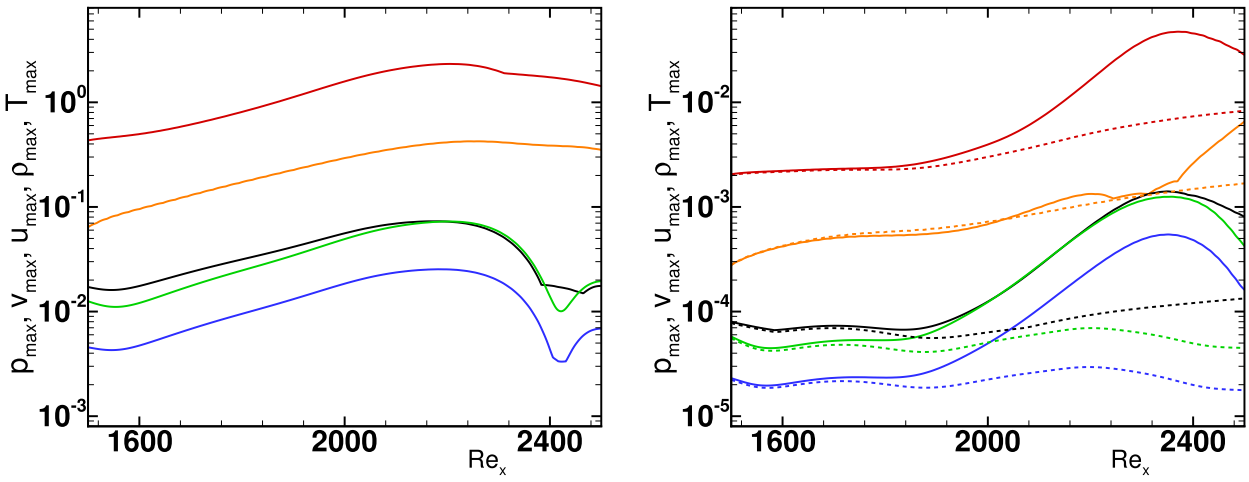

Figure 2: Maximum amplitudes for all velocity components ($A_v^{(1,0)} = 10^{-2}$, $A_v^{(1,\pm k)} = 10^{-4}$, $\Delta\Phi = \pi/4$): Results for component T, ρ, u, v, p (from top to bottom). Left: Fourier mode $(1,0)$. Right: Fourier mode $(1,\pm 4)$, together with linear results (thin dotted lines), which are given for reference.

2, right). The density amplitude for oblique waves grows strongly at the wall (not shown), where it exactly follows the behavior of the pressure disturbance due to the isothermal condition at the wall for the disturbance. The density amplitude maximum is located further away from the wall and it increases only moderately, unlike the behavior seen for all other components.

Figure 3 depicts amplitude functions for the primary disturbance at a streamwise location where secondary amplification can be observed. Corresponding amplitude functions for the secondary disturbance are given in figure 4. The amplitude functions for the secondary disturbance confirm that most of the activity is concentrated near the wall. The overall maximum for the streamwise velocity amplitude is located close to the wall, unlike for linear results given as dotted lines in the figure. Such a behavior could also be seen in figure 14 of Ref. [17]. While the temperature maximum for the secondary disturbance (figure 4, right) is still located away from the wall, the near-wall maximum is not much smaller, again unlike for linear results.

2.2 Subharmonic and Fundamental Resonance

For a thermally perfect gas with wall cooling, Ref. [20] investigates the fundamental resonance of a boundary layer at Mach 10 in the presence of a large-amplitude two-dimensional wave. Figure 5(left) shows both the primary two-dimensional mode $(1,0)$ as well as several oblique fundamental secondary modes with varying spanwise wave numbers k. Similarly, figure 5(right) shows the primary two-dimensional mode $(1,0)$ as well as several oblique subharmonic secondary modes with varying spanwise wave numbers k. The subharmonic modes possess half the frequency of the primary disturbance. Although it can not be directly seen from a comparison of the two plots shown in the figure due to slightly different amplitudes of the primary wave, it was found that the amplification of subharmonic modes is somewhat lower than that for fundamental modes for the setup under consideration here. Therefore, below we focus on the case of fundamental resonance.

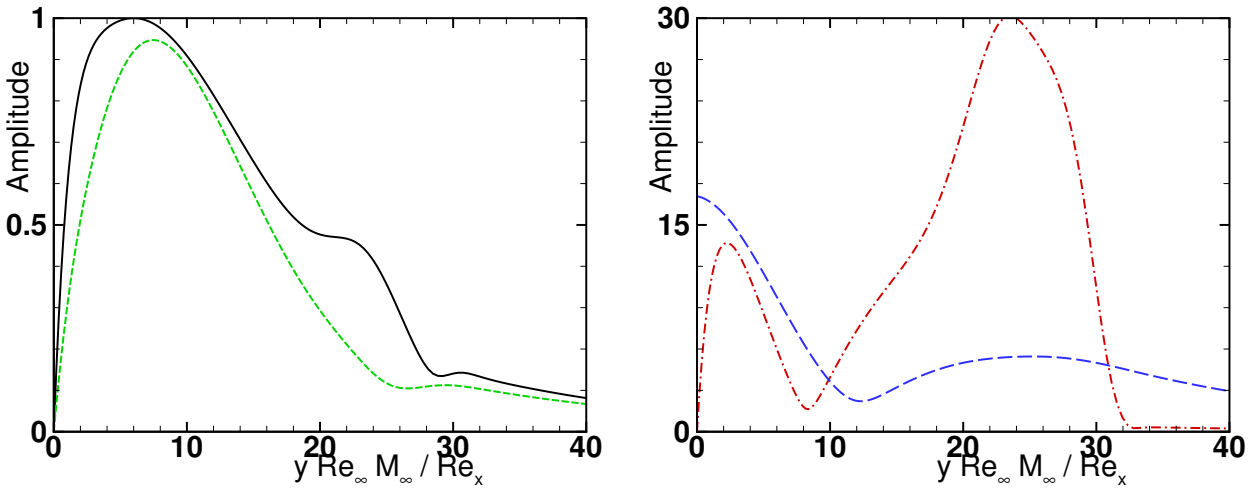

Figure 3: Amplitude functions for mode $(1, 0)$ at Re_x=2122, all normalized by the maximum amplitude of the streamwise velocity component. Left: Streamwise u (solid line) and wall-normal v (dotted line) velocity components. Right: pressure $5\,p$ (dashed line) and temperature T (dash-dotted line).

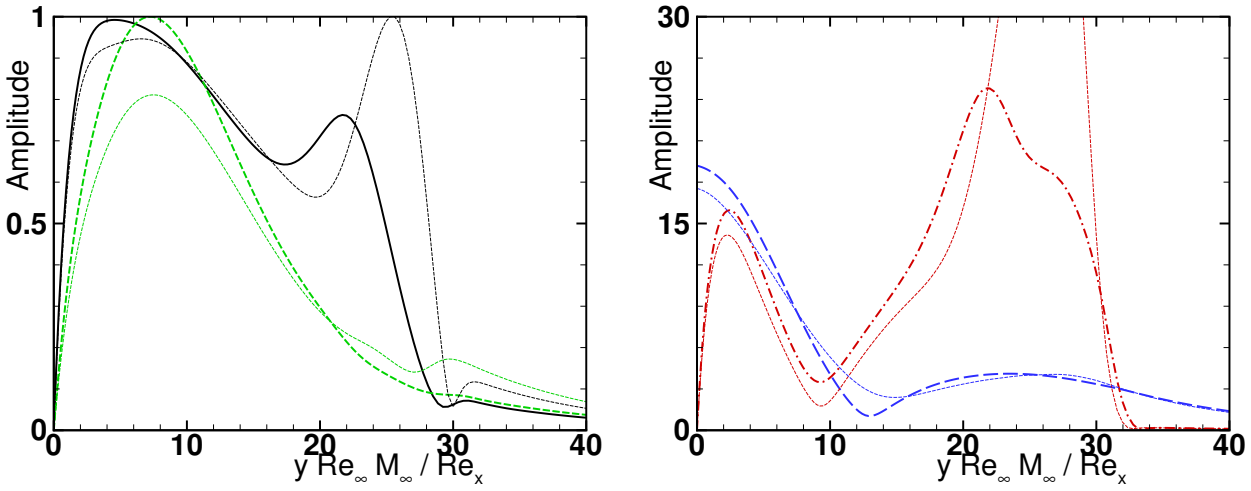

Figure 4: Amplitude functions for mode $(1, \pm 4)$ at Re_x=2122, all normalized by the maximum amplitude of the streamwise velocity component. Left: Streamwise u (solid line) and wall-normal v (dotted line) velocity components. Right: pressure $5\,p$ (dashed line) and temperature T (dash-dotted line). Linear results are given for references as small dotted lines.

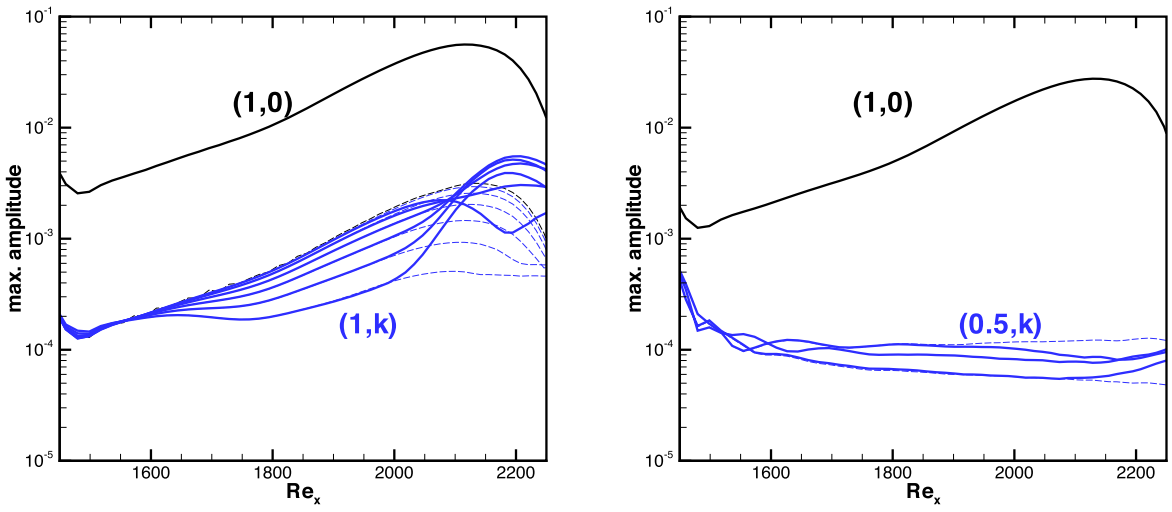

Figure 5: Secondary instability for thermally perfect gas flow with wall cooling. Maximum amplitudes of the streamwise velocity ($A_v^{(1,0)}$, $A_v^{(h,\pm k)}$). Left: for the case of fundamental resonance $h = 1$ [see Ref. 20]. Right: for the case of subharmonic resonance $h = 0.5$.

2.3 Parametric Effects

The growth rate for secondary instability strongly depends on several parameters, including the spanwise wave number k of the secondary perturbation, the amplitude of the primary wave as well as the relative phase difference $\Delta\Phi$ between the primary and the secondary wave [10]. These effects are discussed in the following.

2.3.1 Spanwise Wave Number

The secondary growth rate for fundamental resonance depends primarily on the spanwise wave number of secondary oblique waves. Figure 6 depicts the streamwise evolution of secondary perturbations, modes $(1, \pm k)$ for several different spanwise wave number coefficients k. Largest amplitudes are reached for an intermediate spanwise wave number, which would only be weakly amplified, or not amplified at all, due to a primary instability.

2.3.2 Amplitude of the Primary Wave

When the amplitude of the primary wave mode $(1, 0)$ is reduced, the secondary amplification also decreases. A reduction of primary amplitude by a factor of two compared to what has been considered above (from $A_v^{(1,0)} = 10^{-2}$ down to $A_v^{(1,0)} = 5 \times 10^{-3}$) significantly reduces the secondary growth for both spanwise wave numbers as shown in figure 7, and a further reduction causes the oblique waves to behave linearly again, except for $Re_x > 2300$. This effect occurs for all spanwise wave numbers (compare left and right plots in the figure 7).

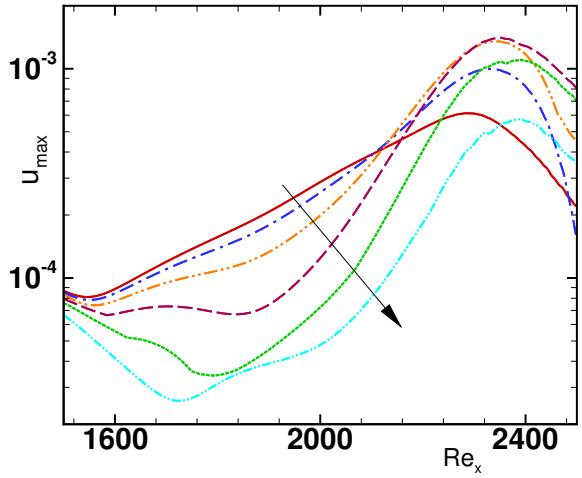

Figure 6: Maximum amplitudes of the streamwise velocity (forcing with $A_v^{(1,0)} = 10^{-2}$, $A_v^{(1,\pm k)} = 10^{-4}$, $\Delta\Phi = \pi/4$) for frozen flow [19]. Results for modes $(1, \pm k)$ with $k = 1 \ldots 6$ (from top to bottom as indicated by the arrow).

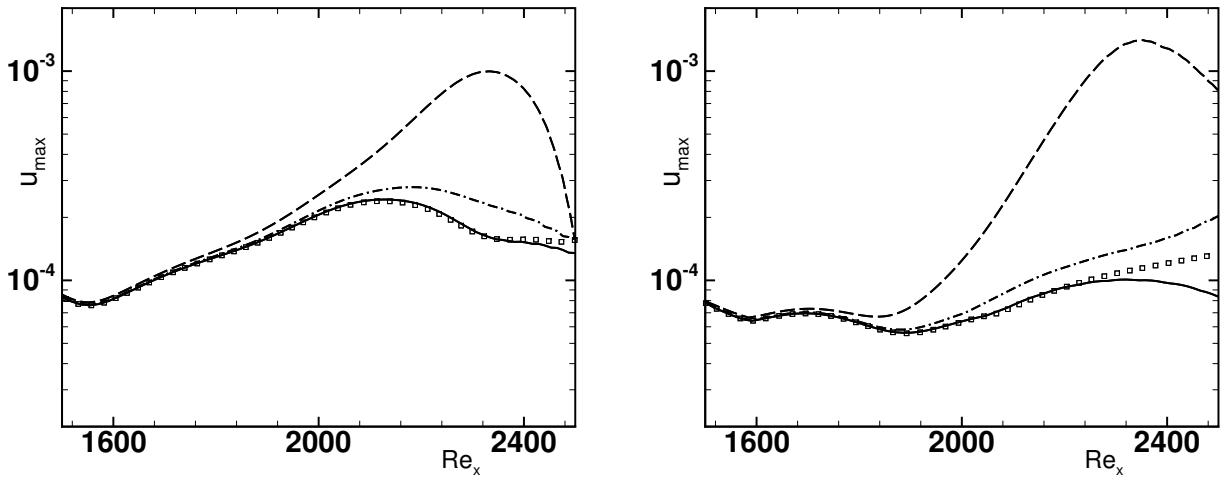

Figure 7: Secondary mode $(1, \pm k)$ amplitudes ($A_v^{(1,\pm k)} = 10^{-4}$, $\Delta\Phi = \pi/4$) for different forcing amplitudes of the primary wave, mode $(1, 0)$: $A_v^{(1,0)} = 10^{-2}$ (dashed line), $A_v^{(1,0)} = 5 \times 10^{-3}$ (dash-dotted line), $A_v^{(1,0)} = 2 \times 10^{-3}$ (solid line). Linear results ($\circ$) are given for reference. Spanwise wave number coefficient $k = 2$ (left) and $k = 4$ (right).

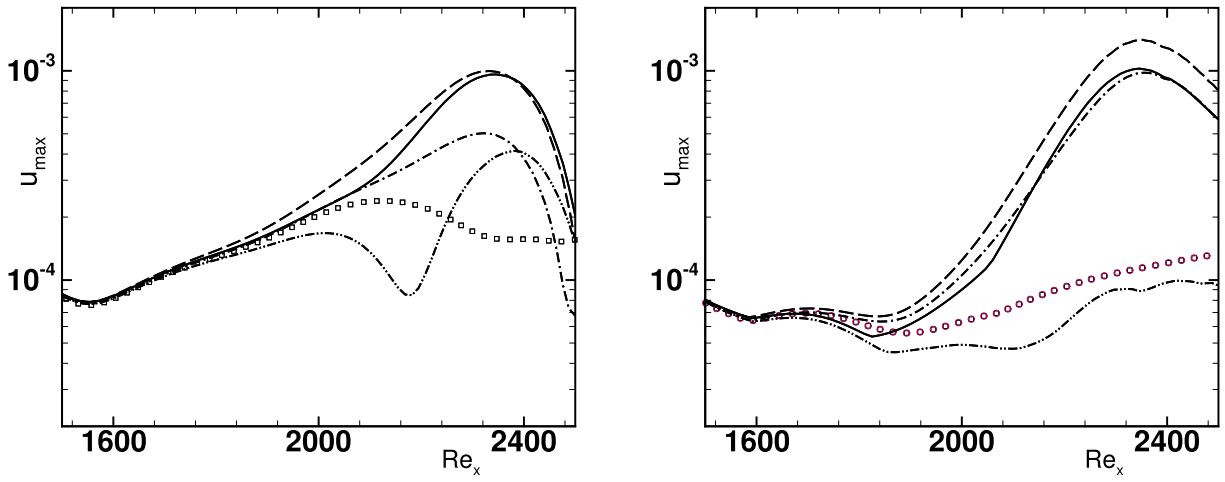

Figure 8: Same as figure 7, but for for several phase differences between the primary ($A_v^{(1,0)} = 10^{-2}$) and the secondary waves: $\Delta\Phi = 0$ (solid line), $\Delta\Phi = \pi/4$ (dashed line), $\Delta\Phi = \pi/2$ (dash-dotted line), $\Delta\Phi = 3\pi/4$ (dash-dot-dotted line). Coefficient $k = 2$ (left) and $k = 4$ (right).

2.3.3 Relative Phase between Primary and Secondary Wave

During secondary instability, the primary and secondary waves fall into resonance [10]. Therefore, the relative phase difference $\Delta\Phi$ between the former and the latter waves is important. We have varied the phase difference between modes $(1, 0)$ and $(1, \pm k)$ through changing the phase $\Phi_0^{(1,\pm k)}$ for a fixed $\Phi_0^{(1,0)}$ in the disturbance forcing strip placed close to the inflow boundary in the simulations. Figure 8 presents results for $k = 2$ (left) and $k = 4$ (right). For a relative phase difference of $\Delta\Phi = \pi/4$, maximum amplification can be observed for both spanwise wave numbers. For a phase difference of $\Delta\Phi = 3\pi/4$, the amplification lies below the value observed in the absence of the primary wave. For $k = 2$ and $\Delta\Phi = 3\pi/4$ (dash-dot-dotted line in figure 8, left), a beating can be seen for $Re_x > 2000$. Ref. [17] found evidence that at least two different eigenmodes, most likely modes F and S [for a definition of these modes, see Ref. 28], are present and participate in the resonance mechanism. The presence of multiple modes could explain the beating and one could apply a multimode decomposition [29] in order to confirm this conjecture. For $k = 2$ (figure 8, right), the amplification rates are different for each phase difference in the range $Re_x \in [2100, 2350]$, indicating that the correct phase relation for full resonance is not easily attained via an adjustment of the phase speeds of the secondary waves.

2.4 The Effect of Freestream Temperature

In Ref. [1] it has been discussed that the freestream temperature has a strong influence on both the base-flow profile as well as primary instability. It was found that the effect of increasing the freestream temperature is analogous to that of wall cooling for both a frozen and a chemically reacting gas. It was further seen that this causes an increase of primary amplification. Larger growth rates eventually lead to larger amplitudes of the two-dimensional wave downstream, and since secondary instability depends on the primary amplitude as discussed in § 2.3.2, we expect that it also leads to stronger secondary amplification. For a frozen gas, such an increase in amplification can indeed be seen for fundamental secondary instability, when increasing $\tilde{T}_\infty$ from $350\,K$ to $425\,K$ (figure 9).

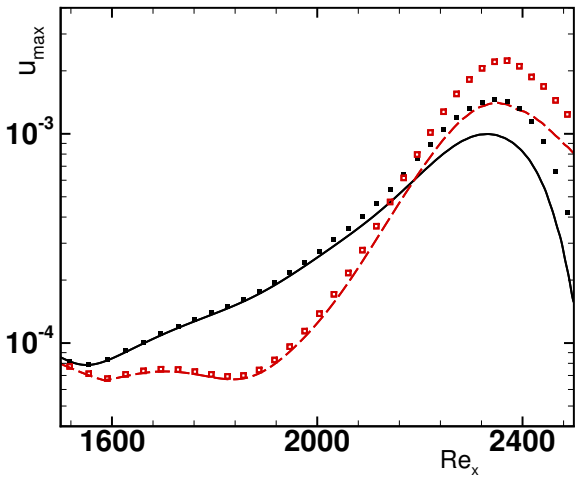

Figure 9: Results for two different freestream temperatures (lines: $\tilde{T}_\infty = 350\,K$, symbols: $\tilde{T}_\infty = 425\,K$). Secondary amplification for a frozen gas (forcing as in figure 6) of modes $(1, \pm k)$, but for $k = 2$ (solid line,•), $k = 4$ (dashed line,□).

2.5 The Effect of Finite-Rate Chemical Reactions

Chemical dissociation reactions occurring mainly close to the wall in the boundary layer, as it happens for the setup considered here, exert a similar effect as cooling at the wall or as increasing the freestream temperature as just discussed in § 2.4 [see also Ref. 1]. Hence, we can expect a very similar effect on the secondary instability as seen in the previous section. Indeed, almost exactly the same difference of secondary amplification rate can be seen between the frozen and the chemically reacting flow at fixed $\tilde{T}_\infty = 350\,K$ (figure 10), as it occurs for a frozen gas when the freestream temperature is increased from $\tilde{T}_\infty = 350\,K$ to $\tilde{T}_\infty = 425\,K$ (figure 9).

These findings suggest that chemical reactions directly increase the primary amplitude but hardly influence the secondary instability mechanism itself. Hence, if the primary amplitude is the same, then secondary amplification will be the same independent of whether the flow is frozen or reacting at a finite rate. This conclusion is expected to hold for moderately reacting flows with finite-rate reactions as they have been considered here, but not necessarily for those in local thermodynamic equilibrium. Also, it may not be valid for setups with high temperature in the freestream and low temperature new the wall due to wall cooling, as they are occur for blunt bodies.

3.0 STRONGLY NON-LINEAR DISTURBANCE EVOLUTION

In order to investigate strongly non-linear effects, we only consider the case of a frozen flow. The excitation amplitude of secondary perturbations was increased from $A_v^{(1,\pm k)} = 1\times10^{-3}$ to $A_v^{(1,\pm k)} = 4\times10^{-3}$ and further to $A_v^{(1,\pm k)} = 8 \times 10^{-3}$. In addition to the primary two-dimensional wave, only a single oblique disturbance with $k = 4$ was forced in the cases with increased forcing amplitude.

As a result of such an increase of secondary amplitude, the secondary disturbances reach an amplitude comparable to that of the primary perturbation (figure 11). We also observe increasingly strong streamwise density gradients. Indirect evidence for the formation of shocklets during the strongly non-linear stage of transition has also been found [19]. Evidence for this latter finding is based on the observation that results could only be obtained when a numerical shock-capturing scheme had been used as the simulation would not

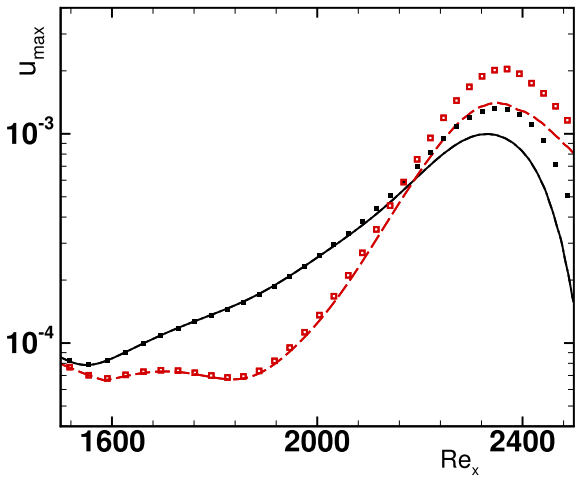

Figure 10: Secondary amplification of modes $(1, \pm k)$ for two different gas models, a frozen gas (lines) and a chemically reacting gas (symbols) for $k = 2$ (solid line,•) and $k = 4$ (dashed line,□), case A with $\tilde{T}_\infty = 350\,K$.

converge otherwise.

Strongly non-linear effects reduce the growth of primary (figure 12, left) and secondary perturbations (figure 12, right). These results show that non-linear effects further enhance the growth of a large-amplitude two-dimensional primary wave only if secondary oblique waves do not attain large amplitudes. If the latter do reach a non-negligible amplitude, growth of the primary wave diminishes, which in turn reduces secondary amplification.

ACKNOWLEDGMENTS

The author would like to thank Thierry Magin, von Karman Institute for Fluid Dynamics, Gianluca Iaccarino, Stanford University, and Eric Shaqfeh, Stanford University, for their contributions and collaboration that lead to the research results presented in this manuscript.

REFERENCES

[1] Marxen, O., "Hydrodynamic Stability of Hypersonic Chemically-Reacting Boundary Layers I," *STO-AVT-289 - Multiphysics phenomena analysis on boundary layer stability in hypersonic regime*, VKI lecture series, 2017.

[2] Mack, L. M., "Boundary layer stability theory," Tech. Rep. JPL-900-277-REV-A; NASA-CR-131501, Jet Propulsion Laboratory, NASA, 1969.

[3] Mack, L. M., "Boundary-Layer Linear Stability Theory," Tech. Rep. 709, AGARD Report, Special course on stability and transition of laminar flow, 1984.

[4] Herbert, T., "Parabolized stability equations," *Ann. Rev. Fluid Mech.*, Vol. 29, 1997, pp. 245–283.

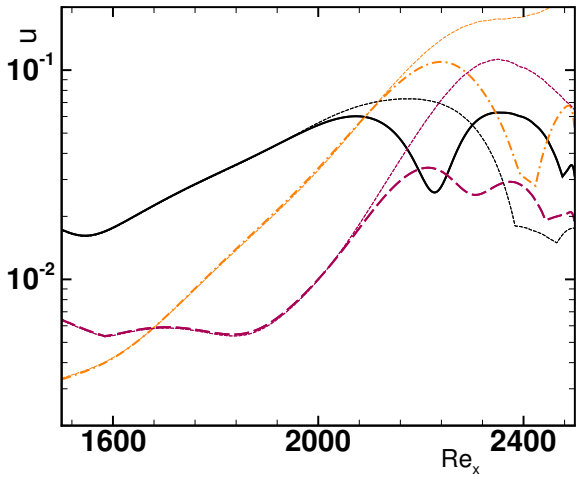

Figure 11: Overview of strongly non-linear results ($A_v^{(1,0)} = 1 \times 10^{-2}$, $A_v^{(1,\pm4)} = 8 \times 10^{-3}$) for frozen gas with shock capturing (lines) for mode $(1, 0)$ (solid line), modes $(1, \pm4)$ (dashed line) and mode $(0, 4)$ (dash-dotted line). Scaled weakly non-linear results are given as dotted lines for reference.

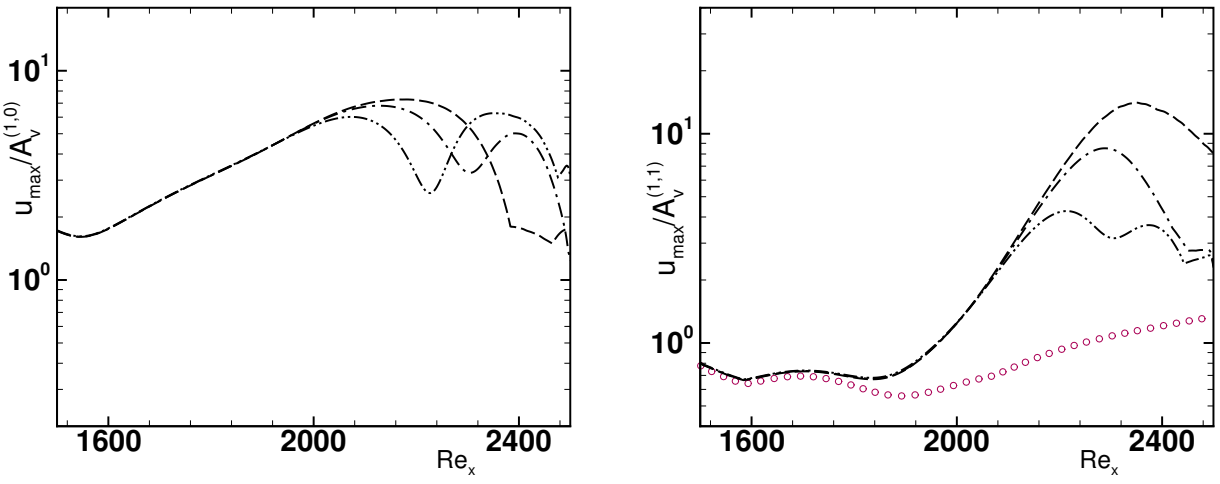

Figure 12: Comparison of results for $A_v^{(1,\pm4)} = 1 \times 10^{-4}$ (dashed line), $A_v^{(1,\pm4)} = 4 \times 10^{-3}$ (dash-dotted line), and $A_v^{(1,\pm4)} = 8 \times 10^{-3}$ (dash-dot-dotted line): mode $(1, 0)$ (left) and mode $(1, \pm4)$ (right). In the right figure, results in the absence of a two-dimensional wave are given for reference (symbols).

[5] Malik, M. R., "Hypersonic Flight Transition Data Analysis Using Parabolized Stability Equations with Chemistry Effects," *J. Spacecraft Rockets*, Vol. 40, No. 3, 2003, pp. 332–344.

[6] Franko, K. J., MacCormack, R. W., and Lele, S. K., "Effects of Chemistry Modeling on Hypersonic Boundary Layer Linear Stability Prediction," *AIAA Paper*, Vol. 2010–4601, 2010.

[7] Chang, C.-L. and Malik, M. R., "Oblique-mode breakdown and secondary instability in supersonic boundary layers," *J. Fluid Mech.*, Vol. 273, 1994, pp. 323–360.

[8] Mayer, C. S. J., von Terzi, D. A., and Fasel, H. F., "Direct numerical simulation of complete transition to turbulence via oblique breakdown at Mach 3," *J. Fluid Mech.*, Vol. 674, 2011, pp. 5–42.

[9] Mayer, C. S. J., Wernz, S., and Fasel, H. F., "Numerical investigation of the nonlinear transition regime in a Mach 2 boundary layer," *J. Fluid Mech.*, Vol. 668, 2011, pp. 113–149.

[10] Herbert, T., "Secondary instability of boundary layers," *Ann. Rev. Fluid Mech.*, Vol. 20, 1988, pp. 487–526.

[11] Mironov, S. G. and Maslov, A. A., "Experimental study of secondary instability in a hypersonic shock layer on a flat plate," *J. Fluid Mech.*, Vol. 412, 2000, pp. 259–277.

[12] Fezer, A. and Kloker, M., "DNS of transition mechanisms at Mach 6.8 – flat plate vs. sharp cone," *West East High Speed Flow Fields 2002*, edited by D. E. Zeitoun, J. Periaux, J. A. Desideri, and M. Marini, Marseille, CIMNE, Barcelona, Spain 2002, 2002, pp. 434–441.

[13] Germain, P. D. and Hornung, H. G., "Transition on a slender cone in hypervelocity flow," *Exp. Fluids*, Vol. 22, 1997, pp. 183–190.

[14] Laurence, S. J., Wagner, A., and Hannemann, K., "Experimental study of second-mode instability growth and breakdown in a hypersonic boundary layer using high-speed schlieren visualization," *Journal of Fluid Mechanics*, Vol. 797, May 2016, pp. 471–503.

[15] Kachanov, Y. S., "Physical Mechanisms of Laminar-Boundary-Layer Transition," *Ann. Rev. Fluid Mech.*, Vol. 26, No. 1, Jan. 1994, pp. 411–482.

[16] Fasel, H., Thumm, A., and Bestek, H., "Direct numerical simulation of transition in supersonic boundary layers: oblique breakdown," *Transitional and Turbulent Compressible Flows*, edited by L. D. Kral and T. A. Zang, ASME-FED, Washington D.C., USA, 1993, pp. 77–92.

[17] Eissler, W. and Bestek, H., "Spatial Numerical Simulations of Linear and Weakly Nonlinear Wave Instabilities in Supersonic Boundary Layers," *Theor. Comp. Fluid Dyn.*, Vol. 8, No. 3, 1996, pp. 219–235.

[18] Marxen, O., Iaccarino, G., and Shaqfeh, E. S. G., "Nonlinear instability of a supersonic boundary layer with two-dimensional roughness," *J. Fluid Mech.*, Vol. 752, July 2014, pp. 497–520.

[19] Marxen, O., Iaccarino, G., and Magin, T., "Direct numerical simulation of hypersonic boundary-layer transition with finite-rate chemistry," *J.Fluid Mech.*, Vol. 755, May 2014, pp. 35–49.

[20] Marxen, O., Magin, T., Iaccarino, G., and Shaqfeh, E. S. G., "A high-order numerical method to study hypersonic boundary-layer instability including high-temperature gas effects," *Phys. Fluids*, Vol. 23, No. 8, 2011, pp. 084108.

[21] Linn, L. and Kloker, M. J., "Investigation of Thermal Nonequilibrium on Hypersonic Boundary-Layer Transition by DNS," *Seventh IUTAM Symposium on Laminar-Turbulent Transition*, edited by P. Schlatter and D. S. Henningson, Vol. 18 of *IUTAM Bookseries*, Proceedings of the Seventh IUTAM Symposium on Laminar-Turbulent Transition, Stockholm, Sweden, 2009, Springer, Berlin, New York, 2010, pp. 521–524.

[22] Kerswell, R. R., "Elliptical Instability," *Ann. Rev. Fluid Mech.*, Vol. 34, 2002, pp. 83–113.

[23] Lagnado, R. R., Phan-Thien, N., and Leal, L. G., "The stability of two-dimensional linear flows," *Phys. Fluids*, Vol. 27, No. 5, 1984, pp. 1094–1101.

[24] Craik, A. D. D. and Criminale, W. O., "Evolution of Wavelike Disturbances in Shear Flows: a Class of Exact Solutions of the Navier-Stokes Equations," *Proc. R. Soc. Lond. A*, Vol. 406, No. 1830, 1986, pp. 13–26.

[25] Berlin, S., Lundbladh, A., and Henningson, D. S., "Spatial simulations of oblique transition in a boundary layer," *Phys. Fluids*, Vol. 6, No. 6, 1994, pp. 1949–1951.

[26] Malik, M. R., "Oblique route to turbulence," *J. Fluid Mech.*, Vol. 674, April 2011, pp. 1–4.

[27] Hudson, M. L., Chokani, N., and Candler, G. V., "Linear Stability of Hypersonic Flow in Thermochemical Nonequilibrium," *AIAA J.*, Vol. 35, No. 6, 1997, pp. 958–964.

[28] Fedorov, A. V., "Transition and Stability of High-Speed Boundary Layers," *Annu. Rev. Fluid Mech.*, Vol. 43, 2011, pp. 79–95.

[29] Tumin, A., Wang, X., and Zhong, X., "Direct numerical simulation and the theory of receptivity in a hypersonic boundary layer," *Phys. Fluids*, Vol. 19, No. 1, 2007, pp. 014101–1–014101–14.